CALIFORNIA PATH PROGRAM
INSTITUTE OF TRANSPORTATION STUDIES
UNIVERSITY OF CALIFORNIA, BERKELEY

Models of Vehicular Collision: Development and Simulation with Emphasis on Safety I: Development of a Model for a Single Vehicle

Oliver M. O'Reilly, Panayiotis Papadopoulos, Gwo-Jeng Lo, Peter C. Varadi

California PATH Research Report
UCB-ITS-PRR-97-15

This work was performed as part of the California PATH Program of the University of California, in cooperation with the State of California Business, Transportation, and Housing Agency, Department of Transportation; and the United States Department of Transportation, Federal Highway Administration.

April 1997

ISSN 1055-1425

Models of Vehicular Collision: Development and Simulation with Emphasis on Safety
I: Development of a Model for a Single Vehicle

REPORT – October 1996

Submitted to: PATH (MOU 232)

Oliver M. O'Reilly (PI)
Panayiotis Papadopoulos (PI)
Gwo-Jeng Lo
Peter C. Varadi

Department of Mechanical Engineering
University of California, Berkeley

Abstract

The development of a novel model for a single vehicle is outlined in this report. The model uses the theory of a Cosserat point to account for the deformable nature of the vehicle. This theory is supplemented with various developments from vehicle system dynamics, such as suspension and tyre models. The complete set of ordinary differential equations governing the vehicle's motion are presented and numerical simulations of the model under various operating conditions are discussed. Several generalizations of the model presented here are possible, and these are mentioned throughout the report.

Keywords: IVHS America, Vehicle Dynamics, Collision Dynamics, Safety, Computer Simulation, Animation and Simulation

Executive Summary

In this report, a novel model for a single vehicle is developed. The development of the model was prompted by the need for a vehicle model which can be used to study various impact scenarios which may arise in vehicle platoons. In this respect, although the model provides a coarse approximation to the deformations of an actual vehicle, it has the distinct advantage of being relatively cheap to simulate numerically.

The collisions of interest here involve small relative velocities. For instance, where two vehicles bump each other. In this situation it is crucial to determine the effects of the collision on the vehicles' subsequent motion. We emphasize that the vehicle model we develop here is not suited to accidents where the vehicles suffer severe damage.

The model uses a theory of a deformable medium which is known as a Cosserat point to model the deformation of the body of the vehicle. In addition, other elements of the vehicle such as the tyres and the suspension systems are discussed in this report. In particular, a Calspan tyre formula is used to model the road-wheel interactions and the suspension system is assumed to consist of MacPherson struts. These elements combined with the Cosserat point constitute the vehicle model.

The report also presents simulations of the vehicle. These simulations show the behavior of the model when the vehicle's center of mass is moving in a straight line and in a curve. The results of these simulations confirm that the model is physically realistic for normal driving maneuvers. In addition, these simulations serve to illustrate some of the difficulties associated with numerical integrations of the vehicle model's governing equations. These difficulties arise because the system of ordinary differential equations associated with the model is stiff.

The present report is part of a series of intended works on the use of the model developed here. Its contents and developments serve as a foundation for the development of models for platoons of vehicles. Each of the vehicles in the platoon will be modeled using the single vehicle model discussed here. In the sequels to this report, we will outline how collisions between two vehicle models can be detected and simulated.

Contents

1 Introduction

Within the framework of the PATH project, the accurate simulation of a single car or a platoon of several cars during regular driving maneuvers is crucial. These maneuvers include acceleration, braking and cornering. They usually arise in combinations, at various speeds and numerous street and weather conditions. There are several vehicle models available to accommodate these issues (see, e.g., [7], [12] and [27]). Due to their complexity, studies of these models usually center on numerical simulations. Clearly, the more refined a model, the more detailed (and hopefully more accurate) are its predictions of the car dynamics during such extreme driving maneuvers as swerving around an obstacle, hard braking or wheel-lockup. Arguably, the most extreme situation arises when the vehicle is in contact with another object.

The types of impacts of interest in the present work are not large scale car crashes where major damage to the chassis results in severe injuries to the passengers. A typical scenario encompassed by our work is rather the following: Consider two cars traveling at highway speeds (perhaps within a platoon) which contact with a moderate relative velocity. We wish to develop a car model which is able to simulate this situation. Furthermore, it should be able to predict the likelihood that this initial contact will lead either to a major accident or a situation where the vehicles can resume their journey after appropriate steering adjustments.

In the majority of vehicle models, the chassis of the vehicle is assumed to be a rigid body which is connected by a suspension system to four wheels. An obvious advantage of this type of model is its relative simplicity: it only has a few inertia parameters and six generalized coordinates to describe the kinematics of the chassis. All additional modeling efforts center on the suspensions, the steering and braking systems, the powertrain and, most importantly, the tyres. Even models for air resistance and wind gusts may be considered in certain cases.

If the aforementioned impact scenario is to be simulated with a rigid body model, coefficients of restitution need to be introduced. These account for the deformation induced by a collision and specify which portions of the vehicle's momenta are lost during the contact. The time of contact for a model of this type is assumed to be negligible. A definite advantage of this method is that it allows this type of model and the computer codes used for its simulation to be easily amended to encompass collision scenarios. However, the main drawback of this approach lies in the specification of

the restitution coefficients; these may depend on impact parameters such as relative velocities, and must be determined using more elaborate models or experiments.

In reality, the chassis is a continuum which deforms during the impact. It may be modeled using standard methods from continuum mechanics. However, it is difficult to obtain any analytical results from the resulting model and recourse to numerical methods, such as the Finite Element Method, is normally used. Using finite elements, the chassis is subdivided and the resulting components are each modeled using a single element. The behavior of each of these elements is described by a set of ordinary differential equations (ODE's) which are relatively easy to integrate numerically. However, the resulting models tend to be elaborate and, in the context of multi-vehicle platoons, computationally expensive.

In the work presented here, a new modeling approach is used. It is based on the use of the theory of a Cosserat point to model the chassis. This theory was introduced by Rubin [18] and subsequently developed by Green and Naghdi [8, 9].[1] Cosserat (or directed) continua are generalizations of the classic continuum theories. They also find application in rod and shell theories. A Cosserat point models a continuum as a material point and a set of directors (hence the name directed theory). From a simplified point of view, one can say that the material point defines the position of the center of mass of the body, while the directors record its orientation and deformation. The more directors used, the better one can approximate the deformation of the body. Section 2 of this report presents this theory in more detail. For simplicity, we will subsequently restrict ourselves to the case of three directors. This particular theory of a Cosserat point is equivalent to the theory of a pseudo-rigid body (see [4, 5, 6, 13, 20, 21, 22]). The latter theory takes its name from its relation to the theory of a rigid body.

Although it is possible to subdivide the chassis into several Cosserat points in a manner reminiscent of finite elements, it was decided to use a single Cosserat point with three directors as a preliminary model. The kinematics of the resulting chassis model are described by 12 generalized coordinates. This number is higher than that used in a rigid body model, but is lower than the corresponding number for a finite element model. In contrast to the rigid body model, the Cosserat point model is deformable and may be viewed as a model which provides an attractive alternative to the

[1] Related theories were independently established by Cohen [4], Muncaster [13], Cohen and Muncaster [5, 6] and Slawianowski [20, 21, 22].

rigid body and finite element models. The companion report [15] discusses algorithms for studying contact and impact of vehicles modeled as Cosserat points.

We now provide a brief outline of this report. In Section 2, background from the theory of a Cosserat point is recalled. This material provides one of the ingredients for developing the vehicle model for a passenger car in Section 3. In the latter section, details on the chassis, suspension and tyre models are presented. The computer codes and simulation for the model developed in Section 3 are provided in Section 4. The final section of this report, Section 5, outlines both the limitations of the model developed here and how additional effects can be incorporated.

2 Summary of the Theory of a Cosserat Point

Consider a three–dimensional (deformable) body $\mathcal{B}$ in Euclidean three–space. The body is bounded by a surface $\partial\mathcal{B}$. The theory of a Cosserat point was developed by Rubin [18] and Green and Naghdi [8] to provide a model for $\mathcal{B}$. Albeit a precise theory in its own right [8], it can also be motivated as an approximation to the classical theory of continuum mechanics [18]. We choose the latter approach here because of our future purpose of modeling the chassis of a vehicle.

Let us identify the material points of the body $\mathcal{B}$ using a convected coordinate system X^i $(i = 1, 2, 3)$. We will assume that in the fixed reference configuration κ_0 of $\mathcal{B}$ these coordinates are Cartesian. Let $\mathbf{r}^*(X^i, t)$ denote the position vector of a typical particle of $\mathcal{B}$ at time t. We approximate this vector (and hereby define the Cosserat point) by

$$\mathbf{r}^*(X^i, t) = \mathbf{r}(t) + \lambda^N(X^i)\mathbf{d}_N(t) \quad , \quad N = 1, \ldots, K \quad . \tag{1}$$

Note that the summation convention over repeated indices is used. The weighting functions $\lambda^N(X^i)$ depend on the problem under consideration and are chosen accordingly.[2] The time dependent vectors $\mathbf{r}(t)$ and $\mathbf{d}_N(t)$, $(N = 1, \ldots, K)$ are called the position vector of the Cosserat point and the directors, respectively. Clearly, the directors record the motion of the body with respect to $\mathbf{r}(t)$. The deformation gradient $\mathbf{F}$ of the motion of $\mathcal{B}$ is

$$\mathbf{F} = \frac{\partial \mathbf{r}^*}{\partial X^i} \otimes \mathbf{E}_i = \frac{\partial \lambda^N}{\partial X^i}\mathbf{d}_N \otimes \mathbf{E}_i \quad , \quad i = 1, 2, 3 \quad , \tag{2}$$

[2] In particular, the determinant of the deformation gradient defined in equation (2) needs to be positive for all motions.

where the basis vectors $\mathbf{E}_i$ form a fixed orthonormal basis for Euclidean three-space and have the associated Cartesian coordinates X^i. The symbol $\otimes$ in equation (2) denotes the usual tensor product.

A fixed reference configuration of the Cosserat point is defined by the vectors $\mathbf{R}$ and $\mathbf{D}_N$. The velocity and director velocities of the Cosserat point are

$$\mathbf{v} = \dot{\mathbf{r}} \quad , \quad \mathbf{w}_N = \dot{\mathbf{d}}_N \quad , \quad N = 1, \ldots, K \quad , \tag{3}$$

where a superposed dot denotes the time derivative.

From the developments of Rubin [18] and Green and Naghdi [8], we recall the mass conservations, the balance of linear momentum, the K balances of director momentum and the balance of angular momentum:

$$\dot{m} = 0 \quad , \quad \dot{y}^N = 0 \quad , \quad \dot{y}^{MN} = 0 \quad , \tag{4}$$

$$m(\dot{\mathbf{v}} + y^N \dot{\mathbf{w}}_N) = \mathbf{n} \quad , \tag{5}$$

$$m(y^N \dot{\mathbf{v}} + y^{NM} \dot{\mathbf{w}}_M) = \mathbf{l}^N - \mathbf{k}^N \quad , \tag{6}$$

$$\mathbf{d}_N \times \mathbf{k}^N = \mathbf{0} \quad . \tag{7}$$

In these equations, m is the mass of the Cosserat point and y^N, $y^{NM} = y^{MN}$ are its inertia parameters. Given the body's reference mass density function $\rho_0(X^i)$, the values of these terms are calculated as follows:

$$m = \iiint_{\mathcal{P}_0} \rho_0 \, dV \quad , \tag{8}$$

$$my^N = \iiint_{\mathcal{P}_0} \rho_0 \lambda^N \, dV \quad , \tag{9}$$

$$my^{NM} = \iiint_{\mathcal{P}_0} \rho_0 \lambda^N \lambda^M \, dV \quad . \tag{10}$$

Here, $\mathcal{P}_0$ denotes the volume occupied by $\mathcal{B}$ in the reference configuration and $\partial\mathcal{P}_0$ will denote the boundary of this volume. For completeness, we also record the mechanical power of the Cosserat point:

$$P = \mathbf{k}^N \cdot \mathbf{w}_N \quad . \tag{11}$$

In the equations (5) and (6), $\mathbf{n}(t)$ and $\mathbf{l}^N(t)$ are the applied force and the applied director forces, respectively. These are calculated using the following identifications:

$$\mathbf{n} = \iint_{\partial\mathcal{P}_0} \mathbf{p} \, dA + \iiint_{\mathcal{P}_0} \rho_0 \mathbf{b} \, dV \quad , \tag{12}$$

$$\mathbf{l}^N = \iint_{\partial \mathcal{P}_0} \lambda^N \mathbf{p}\, dA + \iiint_{\mathcal{P}_0} \rho_0 \lambda^N \mathbf{b}\, dV \quad . \tag{13}$$

Here, $\mathbf{p}(X^i, t)$ is the Piola-Kirchhoff stress vector[3] and $\mathbf{b}(X^i, t)$ is the body force. It should be noted that the derivation of the balance laws for a Cosserat point presume that the body is subject to a body force density $\mathbf{b}$ and surface tractions $\mathbf{p}$ only.

In equations (6) and (7), $\mathbf{k}_N$ are the intrinsic director forces. Their function is similar to that of a stress tensor in the classical theory of continuum mechanics and constitutive equations for the material response are required. We also note at this point that these constitutive equations are such that they identically satisfy the balance of angular momentum (7);[4] a situation that parallels the symmetry of the Cauchy stress tensor in the classical theory.

If the first Piola–Kirchhoff stress tensor $\mathbf{P}(X^i, t)$ under the motion (1) is known, the intrinsic director forces can be calculated using

$$\mathbf{k}^N = \iiint_{\mathcal{P}_0} \frac{\partial \lambda^N}{\partial X^i} \mathbf{P}\mathbf{E}_i\, dV \quad , \quad i = 1, 2, 3 \quad . \tag{14}$$

Alternatively, for a Green–elastic material, the constitutive relations for the intrinsic director forces can be derived in a direct fashion from a stored energy function[5]

$$\psi(\mathbf{d}_N \cdot \mathbf{d}_M, \mathbf{D}_N \cdot \mathbf{D}_M) \quad , \quad N, M = 1, \ldots, K \quad , \tag{15}$$

as

$$\mathbf{k}^N = m \frac{\partial \psi}{\partial \mathbf{d}_N} \quad . \tag{16}$$

A third alternative is the use of the strain energy function ψ^* from classical continuum mechanics. Here, we substitute for the deformation gradient (2) and integrate ψ^* over the volume of the body:

$$m\psi = \iiint_{\mathcal{P}_0} \rho_0 \psi^*(\mathbf{F}^T \mathbf{F}, X^i)\, dV \ . \tag{17}$$

[3]Note that in the subsequent sections of this report, we will use point forces instead of stress distributions. The integrals are then replaced by summations.

[4]The identical satisfaction of the moment of momentum balance law is attributable to the proper invariance under superposed rigid body motions of the constitutive relations (cf., e.g., O'Reilly [14]).

[5]The functional dependence on the scalar products of the directors is an assumption that is made for invariance requirements under rigid body motion (see [14]).

In the next section, we will use the third approach to derive ψ for the chassis of our vehicle.

We close this section with a brief summary of kinematic constraints (see [26]).[6] We will consider only holonomic constraints ϕ of the form

$$\phi(\mathbf{r}, \mathbf{d}_1, \ldots, \mathbf{d}_K, t) = 0 \quad . \tag{18}$$

This type of constraint occurs whenever a Cosserat point comes into contact with a surface or another Cosserat point. This results in a constraint force $\bar{\mathbf{n}}$ and constraint director forces $\bar{\mathbf{l}}^N$ in addition to the applied forces $\hat{\mathbf{n}}$ and $\hat{\mathbf{l}}^N$ given by (12) and (13), respectively: these quantities are calculated using the assumption[7]

$$\bar{\mathbf{n}} = \gamma \frac{\partial \phi}{\partial \mathbf{r}} \quad , \quad \bar{\mathbf{l}}^N = \gamma \frac{\partial \phi}{\partial \mathbf{d}_N} \quad , \quad N = 1, \ldots, K \quad , \tag{19}$$

where γ is an indeterminate Lagrangian multiplier, that is determined using the equations of motion (5) and (6), the constitutive relations (14) or (16) and the constraint (18).

3 The Vehicle Model

Engineers have invented and improved a variety of solutions for functional elements of the automobile such as the motor, the suspensions or the steering system. There are numerous intricate manners in which these elements are related to each other: a feature which make the modeling and design of a single vehicle an extremely difficult task. In response to this difficulty, problem specific mathematical models and computer codes are used to fine–tune design parameters. In this report, a coarse model of a single vehicle is developed for the purpose of investigating impact scenarios. The model uses the theory of a Cosserat point.

The model developed here has the overall features of a vehicle; however, the emphasis is placed on the development of a chassis model using a Cosserat point. In order to gain some insight into the behavior of this model, several important features of the vehicle model are simplified. The

[6] Material constraints, such as incompressibility, are treated in a related manner. We refer the reader to [26] for details.

[7] The derivation of the constraint forces is based on a normality assumption. For details see Casey [2, 3]

various assumptions and simplifications used are discussed in the appropriate locations and suggestions for future possible improvements are made. These modifications are often purely algebraic in nature.

First, we will present the detailed model of the chassis. The suspensions and the wheels are then discussed. The section ends with a discussion of the road/tyre contact. Despite their obvious influence on the overall dynamics of the car, we do not address the brakes, the steering mechanisms, or the motor. These components are, however, present in the form of steering angles and wheel torques. If desired, algebraic or differential expressions for these quantities can be derived and incorporated later.

We wish to make a few more preliminary remarks considering the environmental setting. The reader will find that any influences due to air drag or weather conditions are absent. Road conditions are also of no present concern to us either. In particular, the road is simply modeled as an infinite horizontal plane, i.e., the often tilted and curved nature of highways is ignored.

3.1 The Chassis

3.1.1 Inertia Parameters

We identify the chassis with the body $\mathcal{B}$ of the previous section and present a model that uses the simplest possible Cosserat point with three directors ($K = 3$) and the weighting functions

$$\lambda^i = X^i \quad , \quad i = 1, 2, 3 \quad . \tag{20}$$

In the reference configuration, we identify the directors with the basis vectors of the Euclidean three–space, i.e.,

$$\mathbf{D}_i = \mathbf{E}_i \quad , \quad i = 1, 2, 3 \quad . \tag{21}$$

The reader is referred to Figure 1 for details on the orientation of the directors.

This type of Cosserat point is also known as a pseudo–rigid body [6] for it relates to a rigid body as follows. Using (1), the motion of the particles of $\mathcal{B}$ is

$$\mathbf{r}^*(X^i, t) = \mathbf{r}(t) + X^i \mathbf{d}_i(t) \quad . \tag{22}$$

From equation (2) we see that the deformation gradient

$$\mathbf{F} = \mathbf{d}_i \otimes \mathbf{E}_i \tag{23}$$

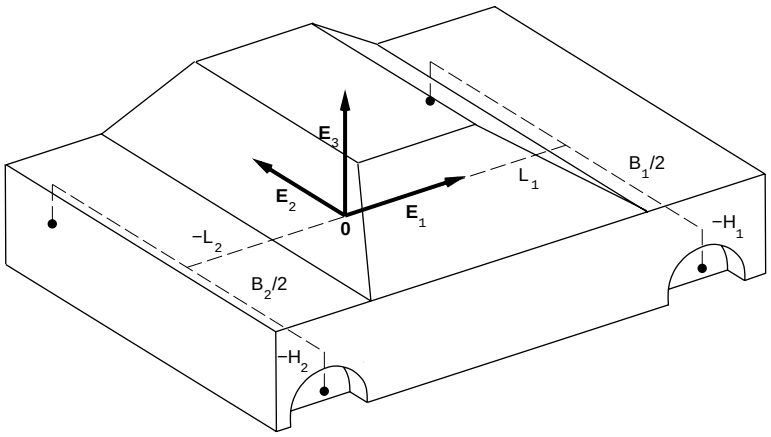

Figure 1: Schematic depiction of the reference configuration of the chassis. The coordinates of the suspension assembly points are also shown in the figure.

is that of a homogeneous deformation. Furthermore, using equation (9), one observes that in the reference configuration, the inertia parameters y^i are the coordinates of the center of mass of the Cosserat point with respect to the position vector $\mathbf{r}$:

$$my^i = \iiint_{\mathcal{P}_0} \rho_0 X^i \, dV \quad . \tag{24}$$

In particular, if we choose $\mathbf{r}$ as the position vector of the center of mass of the chassis,[8] we obtain

$$y^i = 0 \quad . \tag{25}$$

Finally, considering equation (10), we see that the inertia parameters

$$my^{ij} = \iiint_{\mathcal{P}_0} \rho_0 X^i X^j \, dV \tag{26}$$

are in fact the components of the Euler tensor with respect the basis $\{\mathbf{E}_i \otimes \mathbf{E}_j\}$. We recall, from [1], the definition of the inertia tensor $\mathbf{J}_0$ of a rigid body,

$$\begin{aligned} \mathbf{J}_0 &= J_0^{ij} \mathbf{E}_i \otimes \mathbf{E}_j \\ &= \iiint_{\mathcal{P}_0} \rho_0 \left(X^k X^k \mathbf{E}_i \otimes \mathbf{E}_i - X^i X^j \mathbf{E}_i \otimes \mathbf{E}_j \right) dV \quad , \end{aligned} \tag{27}$$

[8] This assumption is intrinsic to the theory of a pseudo–rigid body, see, e.g., [6].

to obtain the following identities

$$my^{ij} = -J_0^{ij} \quad , \quad i \neq j \quad , \tag{28}$$

$$\begin{pmatrix} my^{11} \\ my^{22} \\ my^{33} \end{pmatrix} = \frac{1}{2} \begin{pmatrix} -1 & 1 & 1 \\ 1 & -1 & 1 \\ 1 & 1 & -1 \end{pmatrix} \begin{pmatrix} J_0^{11} \\ J_0^{22} \\ J_0^{33} \end{pmatrix} \quad . \tag{29}$$

Guided by these relations we can obtain the inertia parameters from the data sheets of a specific vehicle.

3.1.2 Constitutive Relations

We are going to derive constitutive relations for the Cosserat point by assuming that all the deformable parts of the chassis are made of the same elastic material with a homogeneous density distribution ρ_0. We hereby ignore any plastic deformations that might occur during an impact.[9]

We proceed by assuming that the chassis consists of a material that, in the classical theory of continuum mechanics, can be described by a nonlinearly elastic, homogeneous, St. Venant–Kirchhoff material with Lamé constants λ and μ and a strain energy function

$$\rho_0 \psi^* = \frac{1}{2} \left(\lambda \, (\mathrm{tr}\mathbf{E})^2 + 2\mu \, \mathbf{E} \cdot \mathbf{E} \right) \quad , \tag{30}$$

where

$$\mathbf{E} = E_{ij} \, \mathbf{E}_i \otimes \mathbf{E}_j = \frac{1}{2} \left(\mathbf{F}^T \mathbf{F} - \mathbf{I} \right) \tag{31}$$

is the standard Lagrangian strain tensor. Here, $\mathbf{I} = \delta_{ij} \, \mathbf{E}_i \otimes \mathbf{E}_j$ is the identity tensor and δ_{ij} denotes the Kronecker symbol. After substituting for the deformation gradient (23), the components of $\mathbf{E}$ become

$$E_{ij} = \frac{1}{2} \left(\mathbf{d}_i \cdot \mathbf{d}_j - \delta_{ij} \right) \quad . \tag{32}$$

Note that $\mathbf{E}$, and therefore also ψ^*, are functions of time only. Hence, the integration of (17) yields

$$m\psi = V \, \rho_0 \psi^* = \frac{V}{2} \left(\lambda \, (\mathrm{tr}\mathbf{E})^2 + 2\mu \, \mathbf{E} \cdot \mathbf{E} \right) \quad . \tag{33}$$

[9] To our knowledge, there is presently no elasto–plastic theory for pseudo–rigid bodies.

The volume V encompasses the entire chassis. We note that the geometry or design of the chassis does not enter the present constitutive relations. However, as deformation gradients become non–homogeneous in future developments of our vehicle model, we will require more detailed data on the composition and geometry of the chassis.

We can now use equation (16) to derive the following expressions for the intrinsic director forces:

$$\mathbf{k}^i = \frac{V}{2}\left(\lambda(\mathbf{d}_j \cdot \mathbf{d}_j - 3)\,\mathbf{d}_i + 2\mu(\mathbf{d}_i \cdot \mathbf{d}_n - \delta_{in})\,\mathbf{d}_n\right) \quad . \tag{34}$$

Finally, for future reference, we record the relations between the Lamé constants and Young's modulus E and Poisson's ratio ν (see [24]):

$$\lambda = E\frac{\nu}{(1+\nu)(1-2\nu)} \quad , \quad \mu = \frac{E}{2(1+\nu)} \quad . \tag{35}$$

3.1.3 Applied Forces

The forces that act on the chassis in our present model are gravity, the suspension forces and the constraint forces during an impact. Once the constraint (18) is known, we can calculate the functional form of the latter forces from (19). We note at this point that for practical reasons, we presently choose an ellipsoid for the outer geometry of the car. The reader is referred to the sequel of this report [15] for further details. Finally, the sole body force acting on the chassis is gravity, i.e.,

$$\mathbf{b} = -g\,\mathbf{E}_3 \quad , \tag{36}$$

where g is the gravitational acceleration.

The suspensions are discussed in the next section. In particular, we will make the assumption that each of the forces $\mathbf{f}^q$ $(q = 1, \ldots, 4)$ due to the four suspensions act at a single point.[10] Using the blue–prints of the vehicle, we record the coordinates (X^1, X^2, X^3) of these four assembly points with respect to the previously defined basis $\{\mathbf{E}_i\}$ (see Figure 1):

$$\left.\begin{array}{lll} 1: & (\ \ L_1\ , & \ \ B_1/2\ , -H_1\ ) \quad \text{left front} \\ 2: & (\ \ L_1\ , & -B_1/2\ , -H_1\ ) \quad \text{right front} \\ 3: & (-L_2\ , & \ \ B_2/2\ , -H_2\ ) \quad \text{left rear} \\ 4: & (-L_2\ , & -B_2/2\ , -H_2\ ) \quad \text{right rear} \end{array}\right\} , \tag{37}$$

[10] In reality, the lateral forces act separately from the vertical forces of the shock absorber.

where B_1 and B_2 are the lateral distances between the two front and two rear wheels, respectively. The assembly points are material points of the chassis and their position vectors $\mathbf{r}_q$ can be calculated from equation (1); e.g., for the right, front suspension,

$$\mathbf{r}_2(t) = \mathbf{r}(t) + L_1\,\mathbf{d}_1(t) - B/2\,\mathbf{d}_2(t) - H_1\,\mathbf{d}_3(t) \quad . \tag{38}$$

Using equations (12) and (13), we can now proceed to calculate the applied force and the applied director forces as follows:

$$\begin{pmatrix} \mathbf{n} \\ \mathbf{l}^1 \\ \mathbf{l}^2 \\ \mathbf{l}^3 \end{pmatrix} = \begin{pmatrix} 1 & 1 & 1 & 1 \\ L_1 & L_1 & -L_2 & -L_2 \\ B_1/2 & -B_1/2 & B_2/2 & -B_2/2 \\ -H_1 & -H_1 & -H_2 & -H_2 \end{pmatrix} \begin{pmatrix} \mathbf{f}^1 \\ \mathbf{f}^2 \\ \mathbf{f}^3 \\ \mathbf{f}^4 \end{pmatrix} - mg \begin{pmatrix} \mathbf{E}_3 \\ y^1\,\mathbf{E}_3 \\ y^2\,\mathbf{E}_3 \\ y^3\,\mathbf{E}_3 \end{pmatrix} . \tag{39}$$

For the gravitational terms we have used the fact that $\mathbf{r}$ is the position vector of the center of mass. We recall that, during an impact, the constraint forces (19) need to be added to $\mathbf{n}$ and $\mathbf{l}^i$ calculated from (39).

3.2 The Suspensions

The suspension of a vehicle connects the wheels to the chassis. It has three main functions; to isolate the chassis from vibrations due to an uneven road surface, to keep the wheels properly aligned and in contact with the road, and to transmit the tyre forces. For practical reasons, independent front suspensions are found in almost all passenger vehicles. They allow a wheel to move vertically without affecting the opposite wheel - which is also advantageous for our modeling purposes. Rear suspensions may also be independent, but one still finds rigid beam axles connecting the rear wheels in some rear wheel driven vehicles.

We start our discussion with independent front suspensions and outline the three basic designs types (see also [7]):

The MacPherson strut is a telescopic member that incorporates a spring and a damping element. At its upper end, it is fixed to the chassis. The kingpin of the wheel is rigidly attached to its lower end. Additional linkages at the lower end transmit the longitudinal and lateral force to the chassis. This configuration is widely used in front wheel driven cars. Since the orientation of the strut with respect to the chassis is constant, this type of suspension can be modeled in a simple manner.

Well adapted to front engine rear wheel driven cars are the A–arm type suspensions. Here, one or two lateral control arms (A–arms) with simple lateral links at each side hold the wheel in place. Between one arm and the chassis, there is a shock absorber. While the arms transmit the lateral and longitudinal tyre forces to the vehicle, they also guide the vertical motion of the wheel. Unlike the MacPherson strut configuration, this motion is not necessarily linear, but follows a curve and the axis of rotation of the wheel may change with respect to the chassis. However, due to the rather simple design, the kinematics of this type of suspension are easily determined. For many purposes it may be sufficient to assume that the wheel motion is rectilinear.

Multi-link suspensions are characterized by ball-joint connections at the end of the linkages. The use of linkages gives the designer freedom to prescribe the six degrees of freedom of the wheel relative to the chassis. Suspensions of this type require substantial modeling efforts to analyze their kinematics.

Given these three concise descriptions, it seems natural to implement the MacPherson strut configuration in our vehicle model. This provides a reasonable approximation for most front suspensions during normal ride and, perhaps, even during the short contact time of an impact. We note however that the additional kinematic features of some front suspensions may become important during corrective maneuvers following the impact.

If we assume a linear spring with coefficient C and a linear damping element with coefficient D, we can calculate a measure of the force generated by the suspension:

$$F_{susp} = C\,(\Delta s - \Delta s_{ref}) + D\,\Delta\dot{s} \quad , \tag{40}$$

where Δs is the distance between the upper and the lower end of the strut and Δs_{ref} is some reference length. This simple model does not account for the nonlinearities of the suspension or for the limitations of the telescope.

If we assume that body roll is moderate, that the radial compliance of the wheels is small (see below), and the road to be horizontal, Δs in the previous equation can be taken as the height over ground of the upper end of the strut (i.e., where the strut connects to the chassis). We will use this simplification in the next section, but the equations can be readily changed if deemed necessary.

Concerning the rear suspensions, one may find a solid drive axle joining the rear wheels in a rear wheel drive car. On it sits the differential with

the drive shaft. The rear suspensions support the axle laterally and absorb shocks vertically. Their kinematics are linked by the rigid rear axle. Sometimes this is modeled by taking the rear axle with the wheels as one body with the suspensions assumed to be independent MacPherson type assembly struts (see, e.g., [10]). The lateral displacements of the tips of the axle due to its rolling are then neglected. This is the model that is used in the work presented here. We are essentially using our aforementioned front suspensions for the rear ones also.

There are designs with independent rear suspensions for both front and rear wheel drive cars. Like the front suspensions discussed above, they use control arm and multi-link configurations. We postpone for future work the decision on whether a MacPherson strut type model is be too simplified for them.

3.3 The Wheels

It is customary to model the whole wheel as a disk, with constant inertia but variable radius (see [16, 7, 27, 12]). That way it behaves essentially like a rigid disk but can account for the radial compliance of the tyre. The kinematics of the wheel are constrained by the road surface and the vehicle suspension.

In order to keep our vehicle model simple, we model each wheel as a mass point with mass m_W. Vertically, the center of each wheel is assumed to stay at a constant distance from the horizontal road surface. Laterally, we assume that the wheels are rigidly attached to a suspension of the MacPherson strut type. Therefore, aside from the tyre forces, the wheels enter the equations of motion (5) and (6) in the form of additional (lateral) inertia parameters that we will derive next. The forces generated in the wheel/road contact are discussed below. Steering forces on the front tyres are assumed to be provided by the steering system and ignored for the time being.

In equation (37), we have defined the coordinates of the four suspension assembly points ($q = 1, \ldots, 4$). Additional assembly points can be introduced when modeling vehicles with more than four wheels. We recall that these points are material points. Hence, we can calculate their velocities $\mathbf{v}_q$ and accelerations $\dot{\mathbf{v}}_q$; e.g., for the right front assembly point (using (38)):

$$\mathbf{v}_2 = \mathbf{v} + L_1\,\mathbf{w}_1 - B/2\,\mathbf{w}_2 - H_1\,\mathbf{w}_3 \quad , \tag{41}$$

$$\dot{\mathbf{v}}_2 = \dot{\mathbf{v}} + L_1\,\dot{\mathbf{w}}_1 - B/2\,\dot{\mathbf{w}}_2 - H_1\,\dot{\mathbf{w}}_3 \quad . \tag{42}$$

We can now split each of the applied forces $\mathbf{f}^q$ into a force $\hat{\mathbf{f}}^q$ and an inertial force $\bar{\mathbf{f}}^q$. The forces $\hat{\mathbf{f}}^q$ consist of the forces due to the shock absorbers and the wheel/road contact. The inertial forces are

$$\bar{\mathbf{f}}^q = -m_W \left((\dot{\mathbf{v}}_q \cdot \mathbf{E}_1)\, \mathbf{E}_1 + (\dot{\mathbf{v}}_q \cdot \mathbf{E}_2)\, \mathbf{E}_2 \right) \quad . \tag{43}$$

This accounts for the facts that the inertial forces of the wheels are only transmitted laterally and that the road is horizontal. Algebraically, we can add the acceleration terms to the left–hand side of the equations of motion (5) and (6), hereby adding additional inertia parameters.

Despite the above assumption of a mass point, we will allow a moment of inertia I_W about the wheel axis so that the wheel can accelerate and brake. By neglecting the radial compliance of the tyres and the remaining moments of inertia, we add only one degree of freedom for each wheel to our system. The additional differential equations are

$$I_W\, \dot{\omega}_q = T^q \quad , \tag{44}$$

where ω_q are the angular velocities of the wheels about the respective wheel axis and T^q are the corresponding applied torques about the axes. If the vehicle under consideration is a rear wheel drive car with rear axle and a differential, then ω_3 and ω_4 are kinematically linked and equation (44) must be modified accordingly.

In order to calculate the forces acting between the tyres and the road surface, it will be necessary to know the orientations of the wheels. The MacPherson type strut suspensions discussed earlier keep the wheels in an upright position. We will assume that the unit heading vectors $\mathbf{h}_{3,4}$ of the rear wheels are parallel to the projection of $\mathbf{d}_1$ into the road plane, i.e.,

$$\mathbf{h}_3 = \mathbf{h}_4 = \frac{(\mathbf{d}_1 \cdot \mathbf{E}_1)\, \mathbf{E}_1 + (\mathbf{d}_1 \cdot \mathbf{E}_2)\, \mathbf{E}_2}{||(\mathbf{d}_1 \cdot \mathbf{E}_1)\, \mathbf{E}_1 + (\mathbf{d}_1 \cdot \mathbf{E}_2)\, \mathbf{E}_2||} \quad , \tag{45}$$

while the unit orientation vectors $\mathbf{a}_{3,4}$ of the rear wheels are perpendicular to $\mathbf{h}_{3,4}$, i.e.,

$$\mathbf{a}_3 = \mathbf{a}_4 = \frac{-(\mathbf{d}_1 \cdot \mathbf{E}_2)\, \mathbf{E}_1 + (\mathbf{d}_1 \cdot \mathbf{E}_1)\, \mathbf{E}_2}{||-(\mathbf{d}_1 \cdot \mathbf{E}_2)\, \mathbf{E}_1 + (\mathbf{d}_1 \cdot \mathbf{E}_1)\, \mathbf{E}_2||} \quad . \tag{46}$$

Similarly, if we define a steering angle Θ about $\mathbf{E}_3$, the unit heading vectors $\mathbf{h}_{1,2}$ and the unit orientation vectors $\mathbf{a}_{1,2}$ of the front wheels are given by

$$\mathbf{h}_1 = \mathbf{h}_2 = \cos\Theta\, \mathbf{h}_{3,4} + \sin\Theta\, \mathbf{a}_{3,4} \tag{47}$$

and

$$\mathbf{a}_1 = \mathbf{a}_2 = -\sin\Theta\, \mathbf{h}_{3,4} + \cos\Theta\, \mathbf{a}_{3,4} \quad . \tag{48}$$

3.4 Wheel/Road Contact

The proper modeling of the forces generated by the tyres is crucial for an accurate vehicle simulation. Analytical models are not feasible due to the tyre's complex design of rubber and steel and its finite deformations during maneuvering of the vehicle. One needs to resort to empirical and semi–empirical methods. We mention here two sources for such models: The Calspan Corporation does extended testing of tyre performance and provides individual curve fitted models of the empirical relationships [25]. The Magic Tyre Model given in [16] provides a set of mathematical formulae from which the tyre characteristics can be calculated. The parameters for these formulae are measured from experiments performed by the Delft University in the Netherlands. Common to these tyre models is the use of terminology. We will recall some (see Figure 2) and refer to [23] for more details. We note in advance that these models do not necessarily apply for combined maneuvers such as combined braking/cornering, even though this is exactly the kind of corrective maneuver one expects following a minor collision between two cars. We postpone the investigation of this problem for future work.

The contact force between the road and the wheel is split as follows: the normal force is normal to the road surface and is generated by the radial compliance of the wheel. Since we have assumed that this compliance is negligible, the normal force is generated directly by the suspension. The longitudinal force acts in the direction of the wheel heading, while the lateral force acts perpendicular to it. Both of these forces act in the road plane.

The wheel camber angle is defined as the angle between the road surface normal and the wheel plane (see Figure 2). When large, e.g., for motorcycles and off-road vehicles, it has considerable influence on the tyre response. Since the suspension of our vehicle model is such that the wheels stay essentially vertical at all times, the camber angle can be neglected. The longitudinal slip is a measure of the difference between the circumferential speed of the wheel and its forward velocity. If they are not equal, a longitudinal friction force is generated. The side slip angle is defined as the angle between the direction of wheel heading and the direction of wheel travel. A non–zero slip angle generates a lateral cornering force.

The aforementioned quantities are sufficient to implement a simple tyre model in the next section. One important addition is related to the tyre's lag dynamics. The lag we are referring to here, is an approximate model for the lateral and longitudinal compliances of the tyre. The presence of these compliances results in a lag of the tyre's response to changes in the side

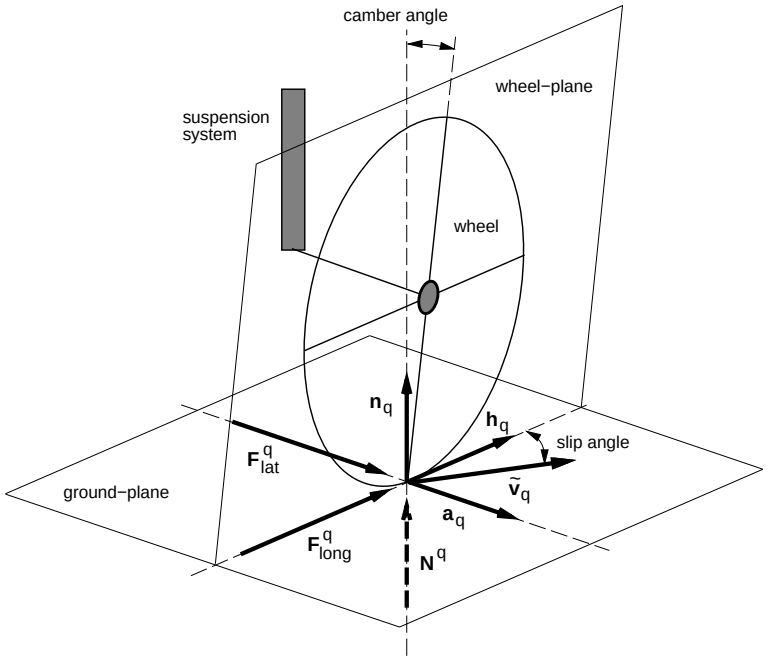

Figure 2: Schematic depiction of one tyre illustrating the forces and kinematic quantities defined in the text. Here, $\mathbf{n}_q$ is the surface normal, such that $\{\mathbf{a}_q, \mathbf{h}_q, \mathbf{n}_q\}$ form a local orthonormal basis. The force $\mathbf{N}^q$ is the normal contact force.

slip angle and longitudinal slip. They imply that the wheel must travel a certain distance, i.e., the wheel must rotate, before the tyre's profile inside the contact patch can adapt to a new situation.

There is yet another, more practical, reason to implement lag dynamics into our model. Since laterally, the wheels are rigidly attached to the deformable chassis, vibrations generated in the chassis can influence the calculations of slip and slip angle directly and may lead to erroneous results. In rigid body vehicle models, this problem is not present. If we introduce lag into our tyre model, these vibrations can be filtered out effectively since the stiffness of the chassis is orders of magnitude higher than the stiffness of the tyre material.

If α denotes the slip angle calculated by the previously indicated method,

then a first–order[11] lagged slip angle response α_{lag} can be calculated from

$$\tau\,\dot{\alpha}_{lag} + \alpha_{lag} = \alpha \quad . \tag{49}$$

This is in fact a low pass filter with a cutoff–frequency τ^{-1} [rad/s] and a unity low–frequency amplification. A similar equation may be derived for the longitudinal slip. We note that this increases the overall order of our vehicle. However, the additional computational effort is minimal when compared to the rest of the vehicle.

4 Implementation of the Vehicle Model

Using the material from previous sections, we derive here the explicit differential equations of our vehicle model. We subsequently outline our implementation of this model in ANSI C and the integration procedure. This section closes with some simulation results for an illustrative example of a vehicle.

4.1 Differential Equations of Motion

We recall that we use are using a Cosserat point with three directors whose position vector is the position vector of the center of mass of the chassis. Besides gravity, suspension forces act at assembly points defined by equation (37). Using equations (25) and (39), the balance equations (5) and (6) may be written in the following form:[12]

$$\begin{pmatrix} m & 0 & 0 & 0 \\ 0 & my^{11} & my^{12} & my^{13} \\ 0 & my^{21} & my^{22} & my^{23} \\ 0 & my^{31} & my^{32} & my^{33} \end{pmatrix} \begin{pmatrix} \dot{\mathbf{v}} \\ \dot{\mathbf{w}}_1 \\ \dot{\mathbf{w}}_2 \\ \dot{\mathbf{w}}_3 \end{pmatrix} = - \begin{pmatrix} \mathbf{0} \\ \mathbf{k}^1 \\ \mathbf{k}^2 \\ \mathbf{k}^3 \end{pmatrix} - \begin{pmatrix} mg\,\mathbf{E}_3 \\ \mathbf{0} \\ \mathbf{0} \\ \mathbf{0} \end{pmatrix} +$$

$$+ \begin{pmatrix} 1 & 1 & 1 & 1 \\ L_1 & L_1 & -L_2 & -L_2 \\ B_1/2 & -B_1/2 & B_2/2 & -B_2/2 \\ -H_1 & -H_1 & -H_2 & -H_2 \end{pmatrix} \begin{pmatrix} \bar{\mathbf{f}}^1 + \hat{\mathbf{f}}^1 \\ \bar{\mathbf{f}}^2 + \hat{\mathbf{f}}^2 \\ \bar{\mathbf{f}}^3 + \hat{\mathbf{f}}^3 \\ \bar{\mathbf{f}}^4 + \hat{\mathbf{f}}^4 \end{pmatrix} . \tag{50}$$

The intrinsic director forces $\mathbf{k}^i$ are given by equation (34). The inertial wheel forces $\bar{\mathbf{f}}^q$ are given by equation (43). For further algebraic manipulations of

[11] Second–order lag models can be used to further improve the tyre response (see [10]).
[12] In writing these equations, $\mathbf{r}$ is chosen such that $y^i = 0$.

equation (50), we define the components of $\mathbf{r}$, $\mathbf{d}_i$, $\mathbf{k}^i$ and $\hat{\mathbf{f}}^q$ with respect to the basis $\{\mathbf{E}_i\}$:

$$
\begin{aligned}
r_j &= \mathbf{r}\cdot\mathbf{E}_j \quad , && (51)\\
d_{ij} &= \mathbf{d}_i\cdot\mathbf{E}_j \quad , && (52)\\
k^i_{.j} &= \mathbf{k}^i\cdot\mathbf{E}_j \quad , && (53)\\
\hat{f}^q_{.j} &= \hat{\mathbf{f}}^q\cdot\mathbf{E}_j \quad . && (54)
\end{aligned}
$$

Subsequently, we introduce the state vector $\mathbf{z}$, the intrinsic force component vector $\mathbf{k}$, a force component vector $\hat{\mathbf{f}}$ and a body force component vector $\mathbf{u}$, i.e.,

$$
\begin{aligned}
\mathbf{z} &= (r_1\,,\, r_2\,,\, r_3\,,\, d_{11}\,,\, d_{12}\,,\, d_{13}\,,\, d_{21}\,,\, d_{22}\,,\, d_{23}\,,\, d_{31}\,,\, d_{32}\,,\, d_{33})^T \ , && (55)\\
\mathbf{k} &= \left(0\,,\, 0\,,\, 0\,,\, k^1_{.1}\,,\, k^1_{.2}\,,\, k^1_{.3}\,,\, k^2_{.1}\,,\, k^2_{.2}\,,\, k^2_{.3}\,,\, k^3_{.1}\,,\, k^3_{.2}\,,\, k^3_{.3}\right)^T \ , && (56)\\
\hat{\mathbf{f}} &= \left(\hat{f}^1_{.1}\,,\, \hat{f}^1_{.2}\,,\, \hat{f}^1_{.3}\,,\, \hat{f}^2_{.1}\,,\, \hat{f}^2_{.2}\,,\, \hat{f}^2_{.3}\,,\, \hat{f}^3_{.1}\,,\, \hat{f}^3_{.2}\,,\, \hat{f}^3_{.3}\,,\, \hat{f}^4_{.1}\,,\, \hat{f}^4_{.2}\,,\, \hat{f}^4_{.3}\right)^T \ , && (57)\\
\mathbf{u} &= (0\,,\, 0\,,\, -mg\,,\, 0\,,\, 0\,,\, 0\,,\, 0\,,\, 0\,,\, 0\,,\, 0\,,\, 0\,,\, 0)^T \ . && (58)
\end{aligned}
$$

Equation (50) can now be written in a Lagrangian second order state space form as

$$
\mathbf{M}\,\ddot{\mathbf{z}} + \mathbf{k}(\mathbf{z}) = \mathbf{A}\,\mathbf{f}(\mathbf{z},\dot{\mathbf{z}},\mathbf{t}) + \mathbf{u} \quad . \tag{59}
$$

The symmetric matrix $\mathbf{M}$ is given by

$$
\mathbf{M} = \begin{pmatrix} \mathbf{M}_{11} & \mathbf{M}_{12} & \mathbf{M}_{13} & \mathbf{M}_{14} \\ \mathbf{M}_{21} & \mathbf{M}_{22} & \mathbf{M}_{23} & \mathbf{M}_{24} \\ \mathbf{M}_{31} & \mathbf{M}_{32} & \mathbf{M}_{33} & \mathbf{M}_{34} \\ \mathbf{M}_{41} & \mathbf{M}_{42} & \mathbf{M}_{43} & \mathbf{M}_{44} \end{pmatrix} \quad , \tag{60}
$$

where M_{qp}, $(q,p = 1,\ldots,4)$ are diagonal three by three sub–matrices. They are listed in Appendix A. The matrix $\mathbf{A}$ is given by

$$
\mathbf{A} = \begin{pmatrix} \mathbf{I} & \mathbf{I} & \mathbf{I} & \mathbf{I} \\ L_1\,\mathbf{I} & L_1\,\mathbf{I} & -L_2\,\mathbf{I} & -L_2\,\mathbf{I} \\ B_1/2\,\mathbf{I} & -B_1/2\,\mathbf{I} & B_2/2\,\mathbf{I} & -B_2/2\,\mathbf{I} \\ -H_1\,\mathbf{I} & -H_1\,\mathbf{I} & -H_1\,\mathbf{I} & -H_1\,\mathbf{I} \end{pmatrix} \quad , \quad \mathbf{I} = \begin{pmatrix} 1 & 0 & 0 \\ 0 & 1 & 0 \\ 0 & 0 & 1 \end{pmatrix} \quad . \tag{61}
$$

We now proceed to calculate the remaining forces $\hat{\mathbf{f}}^q$. We recall the assumption that the suspensions absorb shocks vertically and transmit the tyre forces $\mathbf{f}^q_{tyre}$ laterally, i.e.,

$$
\hat{\mathbf{f}}^q = -F^q_{susp}\,\mathbf{E}_3 + \mathbf{f}^q_{tyre}, \quad , \quad \mathbf{f}^q_{tyre}\cdot\mathbf{E}_3 = 0 \quad , \tag{62}
$$

where F^q_{susp} is given by equation (40). If we admit the simplification that Δs in equation (40) is the height over ground of the assembly point, we obtain, using definitions (37), (51) and (52) and equations (38) and (41),

$$\begin{aligned} F^1_{susp} &= C_1(r_3 + L_1\, d_{13} + B_1/2\, d_{23} - H_1\, d_{33} - \Delta s_{ref,1}) + \\ &\quad D_1(v_3 + L_1\, w_{13} + B_1/2\, w_{23} - H_1\, w_{33}) \quad , \qquad (63) \\ F^2_{susp} &= C_1(r_3 + L_1\, d_{13} - B_1/2\, d_{23} - H_1\, d_{33} - \Delta s_{ref,1}) + \\ &\quad D_1(v_3 + L_1\, w_{13} - B_1/2\, w_{23} - H_1\, w_{33}) \quad , \qquad (64) \\ F^3_{susp} &= C_2(r_3 - L_2\, d_{13} + B_2/2\, d_{23} - H_2\, d_{33} - \Delta s_{ref,2}) + \\ &\quad D_2(v_3 - L_2\, w_{13} + B_2/2\, w_{23} - H_2\, w_{33}) \quad , \qquad (65) \\ F^4_{susp} &= C_2(r_3 - L_2\, d_{13} - B_2/2\, d_{23} - H_2\, d_{33} - \Delta s_{ref,2}) + \\ &\quad D_2(v_3 - L_2\, w_{13} - B_2/2\, w_{23} - H_2\, w_{33}) \quad . \qquad (66) \end{aligned}$$

Here, C_1, D_1, and $\Delta s_{ref,1}$ are the linear spring coefficient, the linear damping coefficient and the spring reference length for the front suspensions, respectively. For the rear suspensions, C_2, D_2, and $\Delta s_{ref,2}$ are the corresponding parameters.

Finally, using definitions (45)–(48), we can decompose the tyre forces $\mathbf{f}^q_{tyre}$ into lateral and longitudinal components with magnitudes F^q_{long} and F^q_{lat}, respectively:

$$\mathbf{f}^q_{tyre} = F^q_{long}\, \mathbf{h}_q + F^q_{lat}\, \mathbf{a}_q \quad . \qquad (67)$$

In order to calculate F^q_{lat}, we will need the side slip angles α_q. For this, using definition (37) and equation (41), we define the direction of wheel travel $\tilde{\mathbf{v}}_q$ to be parallel to the projection of $\mathbf{v}_q$ onto the plane of the road, i.e.,

$$\tilde{\mathbf{v}}_q = \frac{(\mathbf{v}_q \cdot \mathbf{E}_1)\, \mathbf{E}_1 + (\mathbf{v}_q \cdot \mathbf{E}_2)\, \mathbf{E}_2}{||(\mathbf{v}_q \cdot \mathbf{E}_1)\, \mathbf{E}_1 + (\mathbf{v}_q \cdot \mathbf{E}_2)\, \mathbf{E}_2||} \quad , \qquad (68)$$

Using equations (47) and (45), the slip angles are now obtained from

$$\alpha_q = \arctan\left(\frac{(\mathbf{h}_q \times \tilde{\mathbf{v}}_q) \cdot \mathbf{E}_3}{\mathbf{h}_q \cdot \tilde{\mathbf{v}}_q}\right) \quad \text{(no sum on } q\text{)}. \qquad (69)$$

4.2 Numerical Integration

Simulating the motion of a pseudo–rigid body is numerically expensive compared to rigid body models. The frequencies induced by the elastic deformations require very small time steps during integration. Furthermore, for

a Cosserat point, the balance of director momentum (6) is far stiffer than the balance of linear momentum (5). This is due to the intrinsic director forces $\mathbf{k}^N$. This system of equations represents what is called a 'stiff' ODE [17]. Such systems cause problems when integrated with standard numerical methods and special methods have been devised. In the implementation of our vehicle model however, we use a transformation $\mathbf{T}$ of state space variables

$$\mathbf{h} = \mathbf{T}\,\mathbf{z} \tag{70}$$

between the state vector $\mathbf{z}$ defined in (55) and a new state vector $\mathbf{h}$ to circumvent this problem. We choose the invertible transformation matrix $\mathbf{T}$ in a manner that linearly combines the non–stiff equations with the stiff ones, hereby alleviating the stiffness problem; for example,

$$\mathbf{T} = \begin{pmatrix} \mathbf{I} & \mathbf{I} & \mathbf{I} & \mathbf{I} \\ \mathbf{I} & \mathbf{I} & -\mathbf{I} & \mathbf{I} \\ \mathbf{I} & \mathbf{I} & \mathbf{I} & -\mathbf{I} \\ \mathbf{I} & -\mathbf{I} & \mathbf{I} & -\mathbf{I} \end{pmatrix} \quad , \quad \mathbf{I} = \begin{pmatrix} 1 & 0 & 0 \\ 0 & 1 & 0 \\ 0 & 0 & 1 \end{pmatrix} \quad . \tag{71}$$

Using this transformation, the second order system of differential equations (59) can now be written into the first order form

$$\frac{d}{dt}\begin{pmatrix} \mathbf{h} \\ \dot{\mathbf{h}} \end{pmatrix} = \begin{pmatrix} \dot{\mathbf{h}} \\ \mathbf{T}\mathbf{M}^{-1}\left(-\mathbf{k}(\mathbf{T}^{-1}\mathbf{h}) + \mathbf{A}\,\mathbf{f}(\mathbf{T}^{-1}\mathbf{h}, \mathbf{T}^{-1}\dot{\mathbf{h}}, t) + \mathbf{u}\right) \end{pmatrix} \tag{72}$$

and integrated with a numerical package.

The authors have written an ANSI C compatible [11] program that incorporates a vehicle simulation using the equations derived so far. The integration methods include a fixed step-size algorithm, an adaptive step-size control Runge–Kutta algorithm with third order error control, and the Bulirsch–Stoer method with Richardson interpolation. These algorithms have been adapted from the Numerical Recipes handbook [17].

4.3 Examples

We close this section with two illustrative simulations. In the first example, the vehicle is driving forward in a straight line and we show the decaying oscillations of the directors about their equilibria. In the second example, the vehicle is driving in a curve with a constant steering angle.

The vehicle parameters for these test simulations are partly assumed and partly derived from a Toyota Corolla.[13] This data is listed in Appendix B. A Calspan tyre model was adapted from the ILTIS[14] benchmark in [12]. In that benchmark, the wheels are assumed to roll without longitudinal slip and without longitudinal resistance, i.e.,

$$F^q_{long} = 0 \quad . \tag{73}$$

For this reason, the rotation of the wheels given by equation (44) may be ignored. For each wheel, the lateral tyre forces is given by[15]

$$F_{lat} = \mu_y F_{susp}\, g(\bar{\alpha}) \quad , \tag{74}$$

where μ_y is the tyre sideforce friction coefficient given by

$$\mu_y = (-B_1 F_{susp} + B_3 + B_4 F^2_{susp}) SN \quad . \tag{75}$$

The sideforce shaping function is

$$g(\bar{\alpha}) = \bar{\alpha} - \frac{1}{3}\bar{\alpha}|\bar{\alpha}| + \frac{1}{27}\bar{\alpha}^3 \quad \text{for } |\bar{\alpha}| < 3 \quad , \tag{76}$$

$$g(\bar{\alpha}) = \frac{\bar{\alpha}}{|\bar{\alpha}|} \quad \text{for } |\bar{\alpha}| \leq 3 \quad , \tag{77}$$

where the non–dimensional sideslip angle $\bar{\alpha}$ is calculated using

$$\bar{\alpha} = -\frac{A_1 F_{susp}(F_{susp} + A_2) - A_0 A_2}{A_2 \mu_y F_{susp}} \alpha_{lag} \quad \text{if } (-F_{susp}) <= A_2 \quad , \tag{78}$$

$$\bar{\alpha} = \frac{A_0}{\mu_y F_{susp}} \alpha_{lag} \quad \text{if } (-F_{susp}) > A_2 \quad . \tag{79}$$

For each wheel, the lagged side slip angle α_{lag} is obtained from the differential equation (49). The the numerical values of the tyre parameters A_0, A_1, A_2, B_1, B_3, B_4 and SN, as well as the cutoff–frequency τ^{-1}, are listed in Appendix B. Note that F_{lat} is positive for a positive (lagged) slip angle.

The initial conditions for both simulations are the following:

$$\mathbf{r}(0) = \mathbf{0} \quad , \quad \mathbf{d}_i(0) = \mathbf{E}_i \quad , \tag{80}$$

$$\mathbf{v}(0) = 25\, \mathbf{E}_1\, [\frac{km}{h}] \quad , \quad \mathbf{w}_i(0) = \mathbf{0} \quad , \tag{81}$$

$$\alpha_{q,lag}(0) = 0 \quad . \tag{82}$$

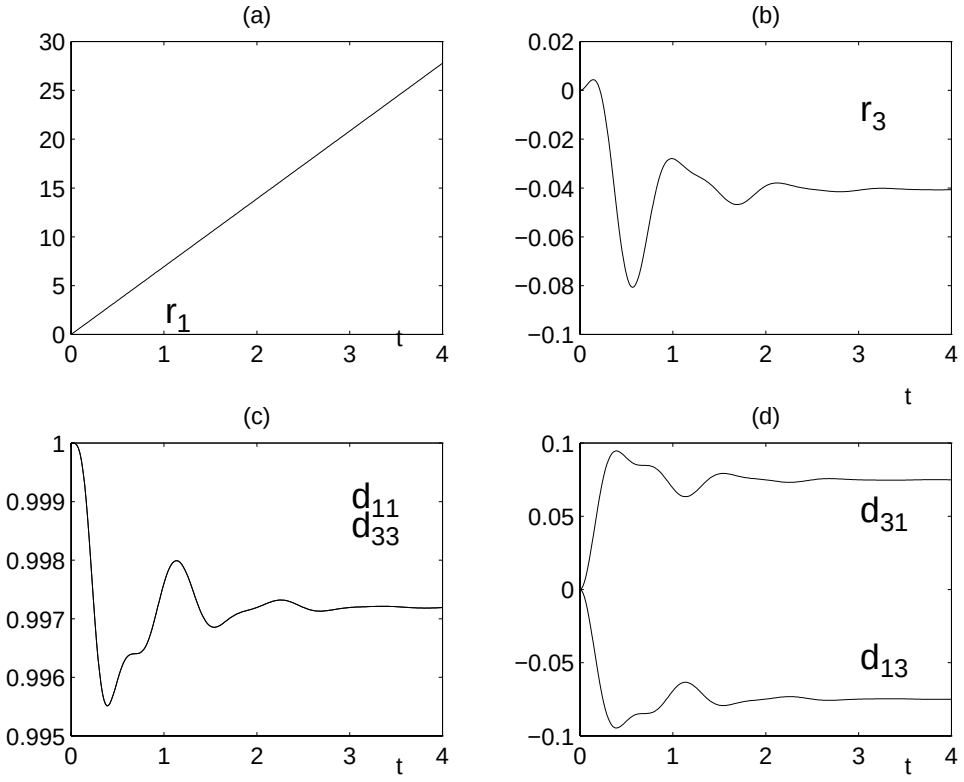

Figure 3: Simulations of a vehicle driving in a straight line for a period of 4 seconds: (a) forward motion of the center of mass, (b) vertical motion of the center of mass, (c) $d_{11}(t)$ and $d_{33}(t)$ (which are practically identical), and (d) $d_{13}(t)$ and $d_{31}(t)$ (which, apart from the sign, are practically identical).

In the first example, the vehicle is driving in a straight line in the direction of $\mathbf{E_1}$, i.e., the steering angle is $\Theta = 0$. The following components of the position vector and the directors are zero (see definitions (51) and (52)):

$$r_2(t) = 0 \quad , \quad d_{12}(t) = d_{21}(t) = d_{23}(t) = d_{32}(t) = 0 \quad . \tag{83}$$

Figure 3a) shows $r_1(t)$ and indicates that the vehicle's center of mass is

[13] Data communicated through Prof. Karl Hedrick, Dept. of Mechanical Engineering, U.C. Berkeley.

[14] The ILTIS is a off–road vehicle. A simplified model of it is used in [12] as a benchmark for the comparison of several vehicle simulation packages.

[15] For readability, we drop the wheel index q.

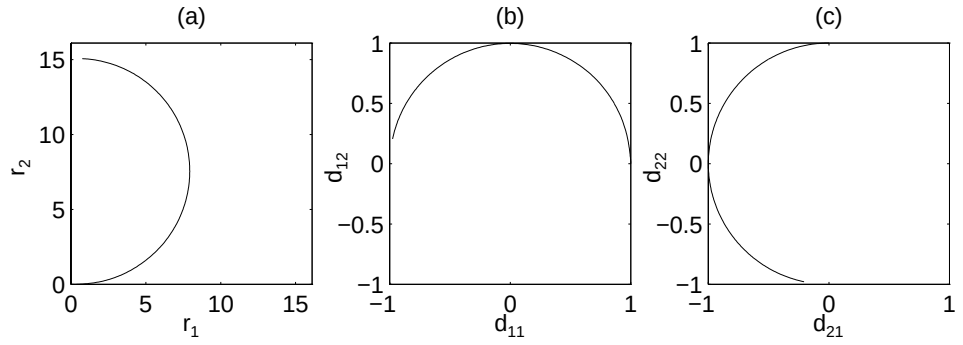

Figure 4: Simulations of a vehicle driving in a curve: (a), (b) and (c) are the respective projections of $\mathbf{r}(t)$, $\mathbf{d}_1(t)$ and $\mathbf{d}_2(t)$ on the road plane during a simulation period of 4 seconds.

moving at a constant speed. Figure 3b) shows $r_3(t)$, i.e., the vertical motion of the vehicle's center of mass. The decaying oscillation about an equilibrium are attributable to the suspensions. The director $\mathbf{d}_2$ oscillates in length without changing its orientation. The magnitude of this oscillation is of the order 10^{-6}. The deformation of the chassis in this example is, as expected, negligibly small. Since the springs in the front suspension systems are softer than those in the rear suspension systems, the vehicle pitches forward in an oscillatory fashion which decays with time. This motion is indicated in Figures 3c) and 3d). Apart from the opposite signs, $d_{13}(t)$ and $d_{13}(t)$ are identical up to high precision and so are $d_{11}(t)$ and $d_{33}(t)$. From this we can conclude that the pitching motion of the vehicle is indeed a rigid body rotation for all practical purposes, i.e., the three directors $\{\mathbf{d}_1, \mathbf{d}_2, \mathbf{b}_3\}$ are almost perfectly orthonormal at all times.

The second simulation shows the vehicle driving with a constant steering angle of twenty degrees, i.e.,

$$\Theta = \frac{\pi}{9}\,[rad] \quad . \tag{84}$$

From Figure 4a) we see that, the curve traced by the projection of $\mathbf{r}(t)$ on the road plane is a circle. Figure 4b) and Figure 4c) show the corresponding projections of the directors $\mathbf{d}_1(t)$ and $\mathbf{d}_2(t)$. This clearly indicates how the car is turning to its left. As in the previous example, the chassis behaves essentially like a rigid body. The vertical motion of the center of mass depicted in Figure 5a) is the same as when the car was going straight (see

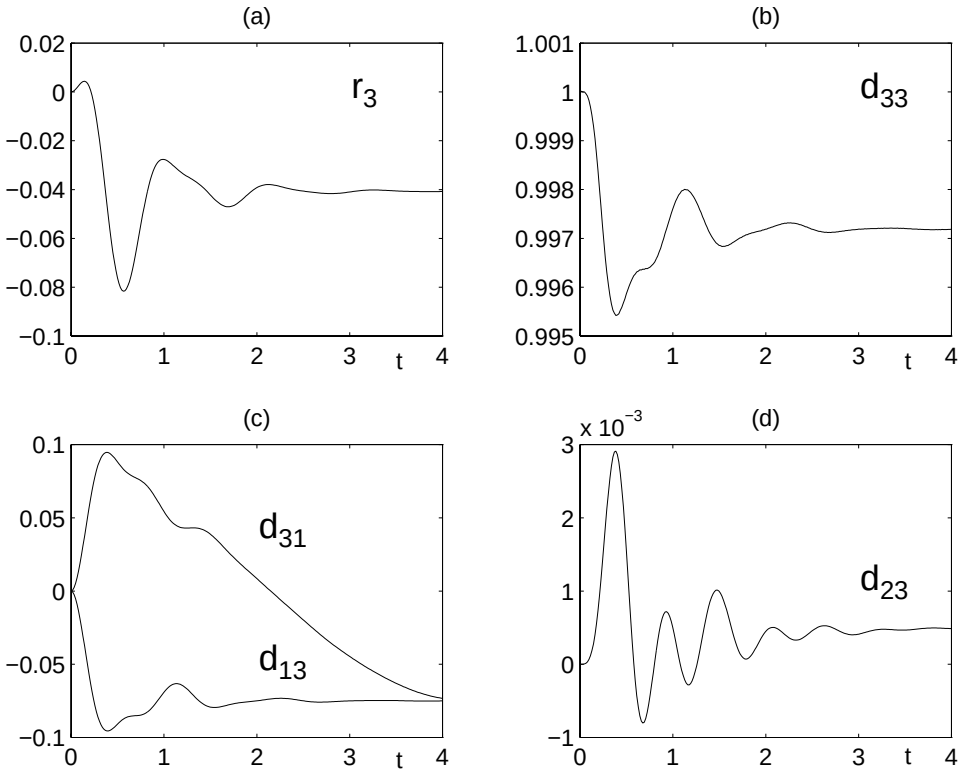

Figure 5: Simulations of a vehicle driving in a curve: (a) vertical motion of the center of mass, (b) d_{33}, (c) d_{13} and d_{31}, and (d) d_{23}. From these figures, (c) indicates that the vehicle is pitching, while (d) indicates that the vehicle is rolling. The simulation period is 4 seconds.

Figure 3b)). The forward roll of the chassis is indicated by $d_{33}(t)$ in Figure 5b) and by $d_{13}(t)$ and $d_{31}(t)$ in Figure 5c). This rolling motion is indeed the same as in the previous example (see Figures 3c) and 3d)) if one observes that $d_{13}(t)$ starts off as the mirror image of $d_{31}(t)$ and, because the vehicle is driving in a circle, gradually changes its sign to become identical with $d_{31}(t)$ towards the end of the simulation. Finally, $d_{23}(t)$ in Figure 5d) indicates that the vehicle is rolling slightly to its right. In reality however, this effect should be much larger that it is indicated by these simulations. We anticipate that improved vehicle parameters and suspension models will remedy this issue.

5 Conclusions

In this report, a model for a single vehicle has been developed and simulated. The model uses the theory of a Cosserat point to account for the deformation of the vehicle. After outlining the theory of a Cosserat point, various developments from vehicle system dynamics were recalled. These developments were then used to complete the vehicle model. Following the presentation of the governing equations for the model in Section 4, a sample of some numerical simulations were presented and discussed. The results of these simulations also served to validate the model: the behavior of the model proved to be physically realistic. The C program which was used for these simulations is available from oreilly@me.berkeley.edu or panos@me.berkeley.edu.

We close this report by referring the reader to the sequel of this report [15]. There, the manner in which vehicle collisions can be studied using the model presented here is discussed. These two reports are part of a series of works aimed at developing models for certain types of collisions which arise in the platooning of vehicles. As mentioned earlier, these models are designed to be suited to modeling impact scenarios where the relative velocities of the vehicles are small.

References

[1] J. Casey. A Treatment of Rigid Body Dynamics. *ASME Journal of Applied Mechanics*, Vol. 50, pp. 905–907, 1983 and Errata, Vol. 51, p. 227, 1984.

[2] J. Casey. Geometrical Derivation of Lagrange's Equations for a System of Particles. *American Journal of Physics*, Vol. 62, No.9, pp. 836–847, 1994.

[3] J. Casey. On the Advantages of a Geometrical Viewpoint in the Derivation of Lagrange's Equations for a Rigid Continuum. *Journal of Applied Mathematics and Physics (ZAMP)*, Vol. 46 (Special Issue), pp. 805–847, 1995.

[4] H. Cohen. Pseudo–rigid Bodies. *Utilitas Mathematica*, Vol. 20, pp. 221–247, 1981.

[5] H. Cohen and R. G. Muncaster. The Dynamics of Pseudo–rigid Bodies: General Structure and Exact Solutions. *Journal of Elasticity*, Vol. 14, pp. 127–154, 1984.

[6] H. Cohen and R. G. Muncaster. *The Theory of Pseudo–rigid Bodies*. Springer Tracts in Natural Philosophy, Vol. 33, Springer Verlag, New York 1988.

[7] T. D. Gillespie. *Fundamentals of Vehicle Dynamics*. Society of Automotive Engineers (SAE), Warrendale, Pennsylvania, 1992.

[8] A. E. Green and P. M. Naghdi. A Thermomechanical Theory of a Cosserat Point with Application to Composite Materials. *Quarterly Journal of Mechanics and Applied Mathematics*, Vol. 44, pp. 335-355, 1991.

[9] A. E. Green and P. M. Naghdi. A Unified Procedure for Construction of Theories of Deformable Media. II: Generalized Continua. *Proceedings of the Royal Society of London, Series A*, Vol. 448, pp. 357–377, 1995.

[10] G. J. Heydinger. Vehicle Dynamics Simulation and Metric Computation for Comparison with Accident Data. DOT HS 807 828, U.S. Department of Transportation, National Highway Traffic Safety Administration, 1991.

[11] B. W. Kernighan and D. M. Ritchie. *The C Programming Language*. 2nd ed., Prentice Hall, 1988.

[12] W. Kortüm and R. S. Sharp, editors. *Multibody Computer Codes in Vehicle System Dynamics*, in *Vehicle System Dynamics*, Vol. 22 Supplement. Swets and Zeitlinger, Amsterdam, 1993.

[13] R. G. Muncaster. Invariant Manifolds in Mechanics II: Zero-Dimensional Elastic Bodies with Directors. *Archives of Rational Mechanics and Analysis*, Vol. 84, pp. 375–392, 1984.

[14] O. M. O'Reilly. A Properly Invariant Theory of Infinitesimal Deformations of an Elastic Cosserat Point. *Journal of Applied Mathematics and Physics (ZAMP)*, Vol. 47, pp. 179–193, 1996.

[15] O. M. O'Reilly, P. Papadopoulos, G. Lo and P. C. Varadi, *Models of Vehicular Collision: Development and Simulation with Emphasis on*

Safety, II: On the Modeling of Collision between Vehicles in a Platoon System. PATH report, 1996.

[16] H. B. Pacejka, editor. *Tyre Models for Vehicle Dynamics Analysis: Proceedings of the 1st International Colloquium on Tyre Models for Vehicle Dynamics Analysis*, in *Vehicle System Dynamics*, Vol. 21 Supplement. Swets and Zeitlinger, Amsterdam, 1991.

[17] W. H. Press, S. A. Teukolsky, W. T. Vetterling and B. P. Flannery, *Numerical Recipes in C: the Art of Scientific Computing.* 2nd ed., Cambridge University Press, 1992.

[18] M. B. Rubin. On the Theory of a Cosserat Point and its Application to the Numerical Solution of Continuum Problems. *ASME Journal of Applied Mechanics*, Vol. 52, pp. 368–372, 1985.

[19] M. B. Rubin. On the Numerical Solution of One-Dimensional Continuum Problems Using the Theory of a Cosserat Point. *ASME Journal of Applied Mechanics*, Vol. 52, pp. 373–378, 1985.

[20] J. J. Slawianowski. Analytical Mechanics of Finite Homogeneous Strains. *Archives of Mechanics*, Vol. 26, pp. 569–587, 1974.

[21] J. J. Slawianowski. Newtonian Dynamics of Homogeneous Strains, *Archives of Mechanics*, Vol. 27, pp. 93–102, 1975.

[22] J. J. Slawianowski. The Mechanics of the Homogeneously–Deformable Body. Dynamical Models with High Symmetries. *Zeitschrift für angewandte Mathematik und Mechanik (ZAMM)*, Vol. 62, pp. 229–240, 1982.

[23] Society of Automotive Engineers. Vehicle Dynamics Terminology: 1978 edn., Warrendale, Pennsylvania, 1978.

[24] I. S. Sokolnikoff. *Mathematical Theory of Elasticity.* 2nd ed., Mc Graw Hill, New York, 1956.

[25] G. A. Tapia. Extended Tire Testing. DOT 6871-V-1, U.S. Department of Transportation, Calspan Corporation, 1983.

[26] P. C. Varadi. *On Cauchy's Lemma and Constraints in the Theory of a Cosserat Point.* Master's Report, Department of Mechanical Engineering, University of California at Berkeley, December 1996.

[27] J. C. Wong. *Theory of Ground Vehicles*. John Wiley and Sons, New York, 1978.

A Components of the Matrix M

This appendix lists the components of the sub–matrices of the matrix $\mathbf{M}$ defined in equation (60):[16]

$$\mathbf{M}_{11} = \mathrm{diag}(m+4m_W\,,\, m+4m_W\,,\, m) \tag{85}$$

$$\mathbf{M}_{22} = \mathrm{diag}\big(my^{11}+2(L_1^2+L_2^2)m_W\,,\, my^{11}+2(L_1^2+L_2^2)m_W\,,\, my^{11}\big) \quad , \tag{86}$$

$$\mathbf{M}_{33} = \mathrm{diag}\big(my^{22}+\tfrac{1}{2}(B_1^2+B_2^2)m_W\,,\, my^{22}+\tfrac{1}{2}(B_1^2+B_2^2)m_W\,,\, my^{22}\big) \quad , \tag{87}$$

$$\mathbf{M}_{44} = \mathrm{diag}\big(my^{33}+2(H_1^2+H_2^2)m_W\,,\, my^{33}+2(H_1^2+H_2^2)m_W\,,\, my^{33}\big) \quad , \tag{88}$$

$$\mathbf{M}_{12} = \mathbf{M}_{21}^T = \mathrm{diag}(2(L_1-L_2)m_W\,,\, 2(L_1-L_2)m_W\,,\, 0) \quad , \tag{89}$$

$$\mathbf{M}_{13} = \mathbf{M}_{31}^T = \mathbf{0} \quad , \tag{90}$$

$$\mathbf{M}_{14} = \mathbf{M}_{41}^T = \mathrm{diag}(-2(H_1+H_2)m_W\,,\, -2(H_1+H_2)m_W\,,\, 0) \quad , \tag{91}$$

$$\mathbf{M}_{23} = \mathbf{M}_{32}^T = \mathrm{diag}\big(my^{12}\,,\, my^{12}\,,\, my^{12}\big) \quad , \tag{92}$$

$$\mathbf{M}_{24} = \mathbf{M}_{42}^T = \mathrm{diag}\big(my^{13}-2(H_1L_1-H_2L_2)m_W\,,\, my^{13}-2(H_1L_1-H_2L_2)m_W\,,\, my^{13}\big) \quad , \tag{93}$$

$$\mathbf{M}_{34} = \mathbf{M}_{43}^T = \mathrm{diag}\big(my^{23}\,,\, my^{23}\,,\, my^{23}\big) \quad . \tag{94}$$

In writing equations (85)–(94), we have used the symmetries $my^{ij} = my^{ji}$.

B Vehicle Parameters

The mass of the vehicle m, the inertia parameters[17] J_0^{ij} and the coordinates of the assembly points L_1,L_2,B_1 and B_2 are derived from a Toyota Corolla, and so are the suspension parameters C_1, C_2, D_1 and D_2. The assembly point coordinates H_1 and H_2 and the spring reference lengths $\Delta s_{ref,1}$ and $\Delta s_{ref,2}$ are assumed:

$$m = 1573.0\ [kg] \quad , \quad \left.\begin{array}{l} J_0^{11} = 479.6 \\ J_0^{22} = 2594.6 \\ J_0^{33} = 2782.0 \end{array}\right\}\ [kg\,m^2] \quad , \quad J_0^{ij} = 0 \quad i \neq j \quad ,$$

[16] $\mathrm{diag}(x, y, z)$ denotes the matrix $\begin{pmatrix} x & 0 & 0 \\ 0 & y & 0 \\ 0 & 0 & z \end{pmatrix}$.

[17] Use equations (28) and (29) to calculate my^{ij}.

$$\left.\begin{array}{l} L_1 = 1.034 \\ L2 = 1.491 \end{array}\right\} \; [m] \quad , \quad B_1 = B_2 = 1.45 \; [m] \quad , \quad H_1 = H_2 = 0 \quad ,$$

$$\Delta s_{ref,1} = \Delta s_{ref,2} = 0.15 \; [m] \quad ,$$

$$\left.\begin{array}{l} C_1 = 17000.0 \\ C_2 = 40000.0 \end{array}\right\} \; [\frac{N}{m}] \quad , \quad \left.\begin{array}{l} D_1 = 1500.0 \\ D_2 = 1200.0 \end{array}\right\} \; [\frac{Ns}{m}] \quad .$$

The gravitational acceleration is

$$g = 9.81 \; [\frac{m}{s^2}] \quad ,$$

and the mass of a wheel is assumed to be

$$m_W = 10.0 \; [kg] \quad .$$

The volume V of the chassis, Young's modulus E and Poisson's ratio ν are assumed to have the values[18]

$$V = 0.42 \; [m^3] \quad , \quad E = 200.0 \cdot 10^6 \; [\frac{N}{m^2}] \quad , \quad \nu = 0.30 \; [.] \quad .$$

Finally, the parameters for the Calspan tyre model given in [12] are

$$A_0 = 2625 \; [N] \quad , \quad A_1 = 14.47 \; [.] \quad , \quad A_2 = 12930 \; [N] \quad ,$$

$$B_1 = -0.464 \cdot 10^{-4} \; [N^{-1}] \quad , \quad B_3 = 1.216 \; [.] \quad , \quad B_4 = 0.218 \cdot 10^{-10} \; [N^{-2}] \quad ,$$

$$SN = 1.0274 \; [.] \quad .$$

The cutoff–frequency τ^{-1} for describing the tyre's lag dynamics is assumed to be

$$\tau^{-1} = 2\pi \cdot 100 \; [rad \, s^{-1}] \quad .$$

[18] The Lamé constants are calculated using (35).